ACS OMEGA

http://pubs.acs.org/journal/acsodf

Article

Effect of Propargylic Substituents on Enantioselectivity and Reactivity in Ruthenium-Catalyzed Propargylic Substitution Reactions: A DFT Study

Ken Sakata,* Yuuri Uehara, Shiona Kohara, Takeshi Yoshikawa, and Yoshiaki Nishibayashi

Cite This: *ACS Omega* 2022, 7, 36634−36642

Read Online

ACCESS | Metrics & More | Article Recommendations | Supporting Information

ABSTRACT: We recently proposed a transition-state model for asymmetric propargylic substitution reactions of propargylic alcohols catalyzed by optically active thiolate-bridged diruthenium complexes [*Chem. − Asian J.* **2021**, *16*, 3760−3766]. In the present study, we further examined the effects of propargylic substituents on both enantioselectivity and reactivity in the propargylic substitution reactions via ωB97X-D-level density functional theory (DFT) calculations. When the propargylic alcohol bears a methyl group at the propargylic position, we obtained results that contrast with the result of our previous study on propargylic alcohols without methyl groups. This result indicates that methyl group substitution at the propargylic position reverses the stereoselectivity. Substitution of a trifluoromethyl group for a methyl group was suggested to result in higher enantioselectivity. The obtained results are consistent with the experimental study on enantioselective propargylic phosphinylation reactions reported by our group.

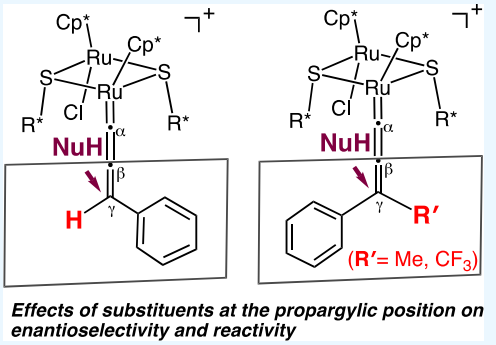

Effects of substituents at the propargylic position on enantioselectivity and reactivity

INTRODUCTION

The catalytic asymmetric propargylic substitution reaction of propargylic alcohols or their derivatives is an efficient tool for constructing a stereocenter at the propargylic position.[1] Since Nishibayashi et al. reported the asymmetric propargylic alkylation reaction of propargylic alcohols with acetone in the presence of an optically active thiolate-bridged diruthenium complex (**1**) (Scheme 1),[2] transition metal- and organocatalyzed enantioselective propargylic substitution reactions have been gradually developed.[3−5]

Scheme 1. Asymmetric Propargylic Substitution Reactions of Propargylic Alcohols with Acetone Catalyzed by Optically Active Thiolate-Bridged Diruthenium Complexes[2]

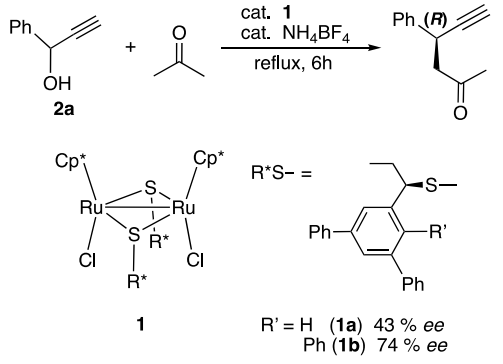

In our previous study, we examined the reaction of ruthenium−allenylidene complex **3a**, which is generated from an optically active thiolate-bridged diruthenium complex $[Cp^*RuCl(SR^*)]_2$ ($Cp^* = \eta^5$-C_5Me_5, SR* = (*R*)-SCH(Et)-$C_6H_3Ph_2$) (**1a**) and 1-phenylprop-2-yn-1-ol (**2a**), with prop-1-ene-2-ol, which is the enol isomer of acetone.[6] We used ωB97X-D-level DFT calculations to clarify the origin of the enantioselectivity in the reaction of **2a** with acetone catalyzed by **1a** or **1b** (Scheme 2). By exploring a variety of transition-state structures for the nucleophilic attack of enol on the γ-carbon (C_γ) atom at the ruthenium−allenylidene complex, we revealed that the number of lower-energy structures leading to the major *R*-product ((***R***)**4a**) is larger than that of the structures leading to the minor *S*-product ((***S***)**4a**), which indicates stereoselectivity in the allenylidene moieties.

A variety of nucleophiles, such as *N*,*N*-dimethylaniline, furan, indole, 1,5-enyne, and 2-naphthol, were experimentally applied for the enantioselective propargylic substitution reactions catalyzed by **1a** or **1b**, and the reactions of **2a** provided the major products that were obtained by the attack of the nucleophiles from the same direction of the allenylidene

Received: July 22, 2022
Accepted: September 22, 2022
Published: October 4, 2022

ACS Publications

© 2022 The Authors. Published by American Chemical Society

https://doi.org/10.1021/acsomega.2c04645
ACS Omega 2022, 7, 36634−36642

Scheme 2. Examined Reaction Pathway of Ruthenium−Allenylidene Complex 3, Which Is Generated from 1a and Propargyl Alcohol 2, with Prop-1-ene-2-ol

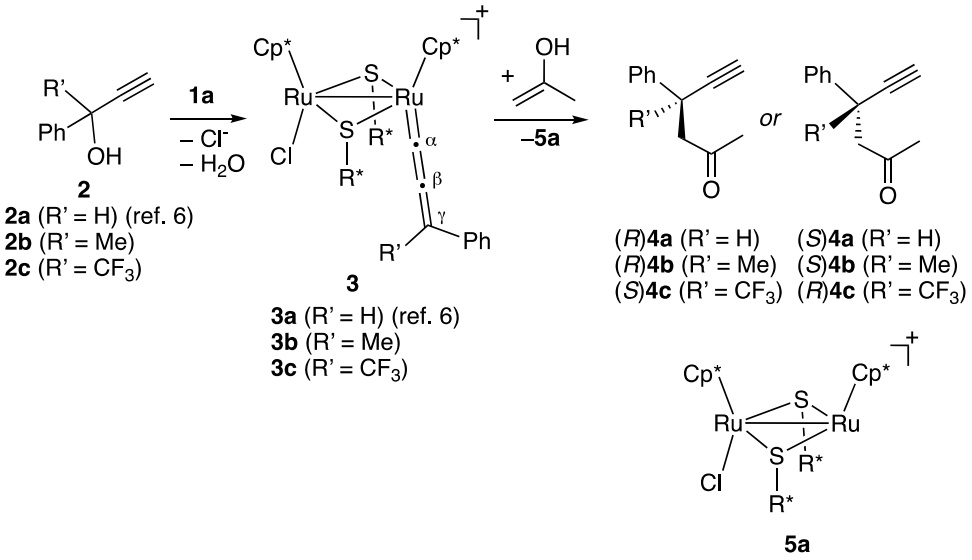

ligand (A-face attack in Scheme 3).[1] However, our group recently reported the diruthenium-catalyzed reaction between

Scheme 3. Definition of the Faces at the C_γ Position of the Allenylidene Ligand in the Present Study[1]

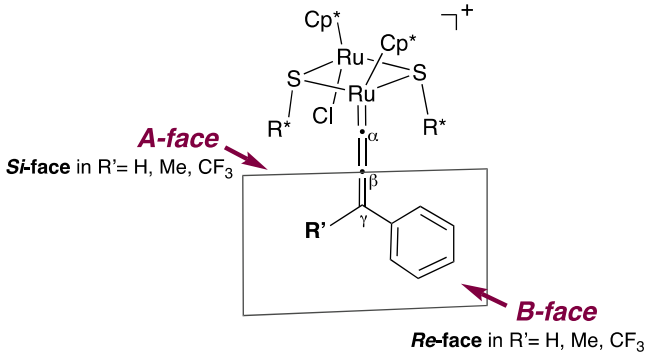

[1]In the cases of R′ = H, CH_3, and CF_3, A- and B-faces correspond to *Si*- and *Re*-faces, respectively.

phosphine oxide and propargylic alcohol bearing a trifluoromethyl group at the propargylic position (**2c**) (Scheme 4)[7] and found the major product obtained by the attack of the nucleophile from the different direction (B-face attack in Scheme 3).

Thus, the effects of propargylic substituents on the stereoselectivity and reactivity of propargylic substitution

Scheme 4. Propargylic Phosphinylation Reaction of Propargylic Alcohol Bearing Trifluoromethyl Groups at the Propargylic Position with Diphenylphosphine Oxide in the Presence of 1a or 1b[7]

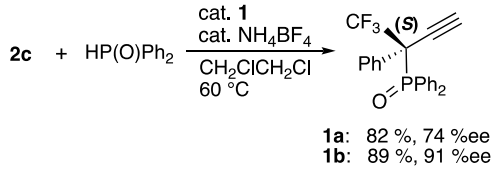

reactions catalyzed by the diruthenium complex **1a** are next target of our studies. Based on findings obtained in our previous DFT studies,[6,8] we, in the present study, examine model propargylic substitution reactions of propargylic alcohols **2b** and **2c** (R′ = Me and CF_3, respectively, in Scheme 2) catalyzed by diruthenium complex **1a**.

RESULTS AND DISCUSSION

Complexes. The ruthenium−allenylidene complex plays an important role as the key intermediate in the diruthenium-catalyzed propargylic substitution reactions.[9,10] For **3a**, six equilibrium structures with weak intramolecular interactions between the terminal phenyl group in the thiolate ligand and the phenyl group in the allenylidene ligand, $\mathbf{I_x}$ (x = a−f), were observed in our previous calculations, and the difference in free energy between these structures was relatively small (Figure 1).[6]

For **3b**, six structures $\mathbf{I_{Mx}}$ (x = a−f) were identified, as was true of **3a** (Figures 1 and S1). Structure $\mathbf{I_{Ma}}$, which has an intramolecular CH/π interaction between the *meta*-C−H bond of the terminal phenyl group of the thiolate ligand and the phenyl group of the allenylidene, corresponds to structure $\mathbf{I_a}$ observed via X-ray crystallography for **3a** (Figure S2 shows the noncovalent interaction (NCI) plot[11]). The distance between the hydrogen atom of the terminal phenyl group of the thiolate ligand and the phenyl ring of the allenylidene is 2.75 Å, which is slightly shorter than that in $\mathbf{I_a}$, 2.80 Å (Figure S1). The structure $\mathbf{I_{Mb}}$ has a $\pi-\pi$ interaction between the terminal phenyl group of the thiolate ligand and the phenyl group of the allenylidene ligand instead of a CH/π interaction. The distance between two phenyl rings is 3.82 Å, which is also shorter than that of $\mathbf{I_b}$, 3.84 Å. These results indicate that the electron-donating methyl group enhances CH/π and $\pi-\pi$ interactions.[12] $\mathbf{I_{Mb}}$ is slightly lower in free energy than $\mathbf{I_{Ma}}$ by 1.2 kcal/mol, showing almost the same energy difference as those in **3a** ($\mathbf{I_b}$ is lower than $\mathbf{I_a}$ by 1.5 kcal/mol; Figure 1). In the $\mathbf{I_{Mc}}$ structure, which corresponds to $\mathbf{I_c}$, the methyl group moves away from the terminal phenyl group of the thiolate ligand, while the C_γ−H bond in allenylidene interacts with the terminal phenyl group of the thiolate ligand in $\mathbf{I_c}$. Thus, the

https://doi.org/10.1021/acsomega.2c04645
ACS Omega 2022, 7, 36634−36642

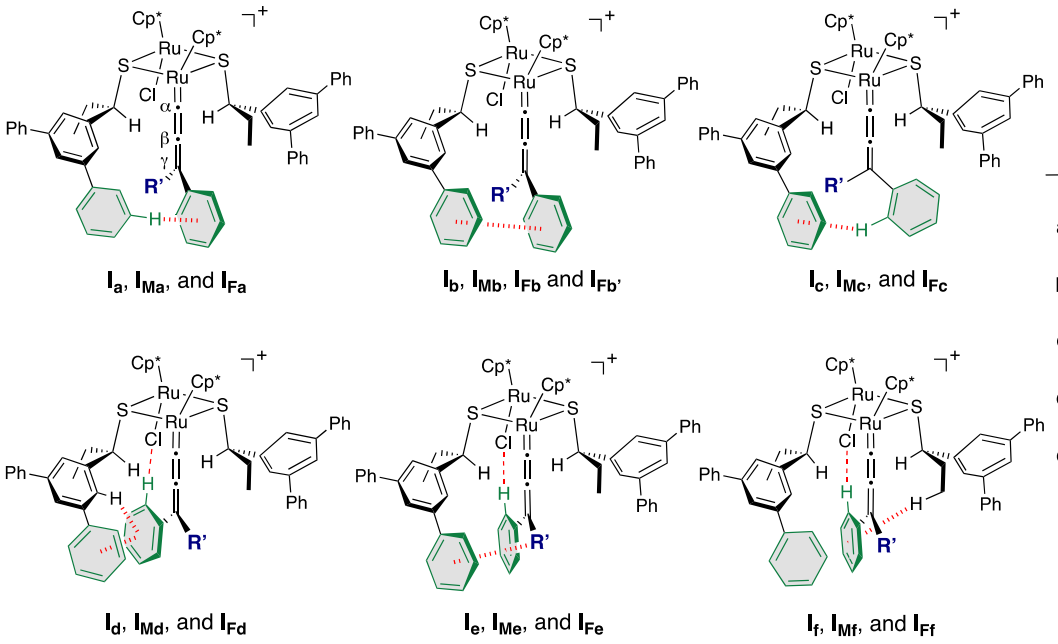

x	I_x (R' = H)	I_{Mx} (R' = Me)	I_{Fx} (R' = CF_3)
a	1.5	1.2	0.6
b	0.0	0.0	0.0, 0.5
c	2.1	3.2	0.2
d	0.5	1.4	-0.7
e	0.1	0.2	-1.3
f	1.5	3.4	0.8

Figure 1. Structures of ruthenium−allenylidene complexes I_x, I_{Mx}, and I_{Fx} for **3a**, **3b**, and **3c**, respectively (x = a−f). The relative Gibbs free energies, $\Delta G^{333\,K}$, are listed (kcal/mol).

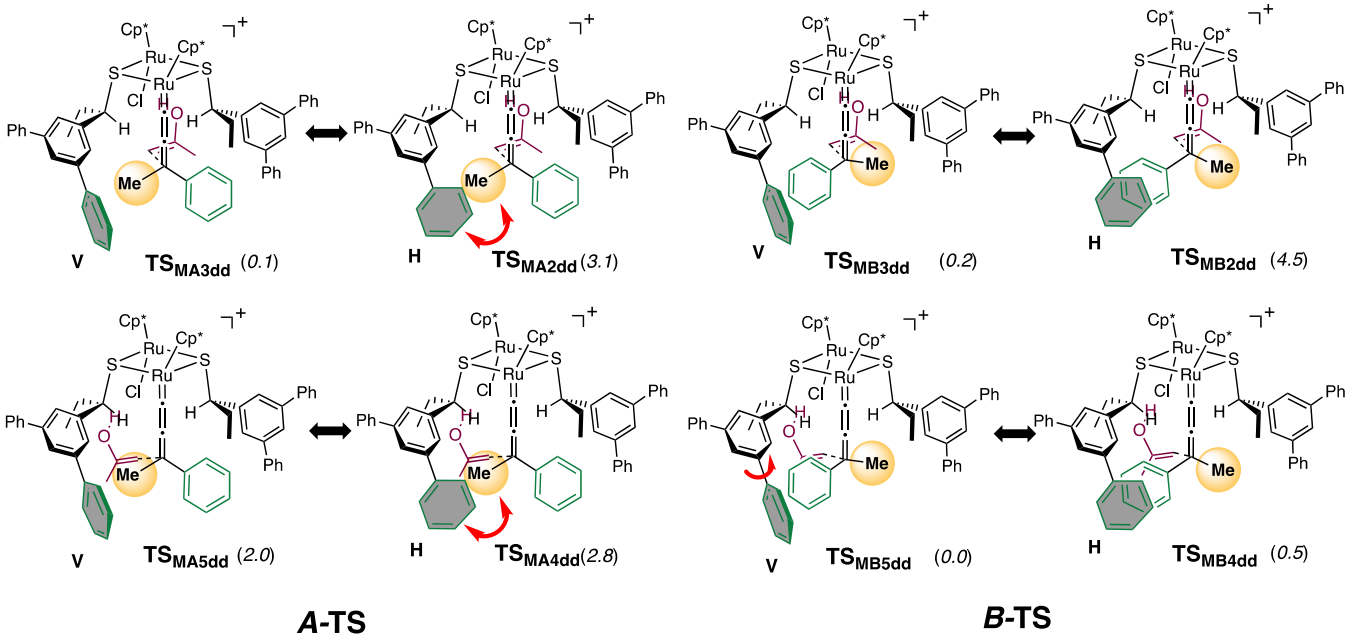

Figure 2. Transition-state structures for the reaction of ruthenium−allenylidene complex **3b**. The Gibbs free energies relative to TS_{MB5dd} at 333 K, $\Delta\Delta G^{333\,K}$, are given in parentheses (kcal/mol).

energy of I_{Mc} relative to I_{Mb}, 3.2 kcal/mol, is higher than that of I_c relative to I_b, 2.1 kcal/mol. In the I_{Md}, I_{Me}, and I_{Mf} structures, meanwhile, the allenylidene moiety is rotated, and the *ortho*-C−H bond in the phenyl group of the allenylidene interacts with the chloride ligand, which coordinates to the ruthenium atom different from the atom attached to the allenylidene ligand. The energies of I_{Md} and I_{Mf} relative to I_{Mb} are 1.4 and 3.4 kcal/mol, respectively, which are slightly higher than the relative energies of **3a** (0.5 and 1.5 kcal/mol), while I_{Me} has almost the same relative energy as I_{Mb} (0.2 kcal/mol). The CH/π interactions between one of the methyl C−H bonds in the allenylidene ligand and the terminal phenyl group in the thiolate ligand and the interactions between the *ortho*-C−H bond of the phenyl group in the allenylidene and the chloride ligand were observed in I_{Me} (Figure S2 for the NCI plot; the distance between the hydrogen atom and the terminal phenyl group in the thiolate ligand is 2.55 Å).[13]

For **3c**, seven equilibrium structures I_{Fx} were obtained because two structures corresponding to the structure I_{Mb}, I_{Fb} and $I_{Fb'}$, were identified (Figures 1 and S1).[14] Among the seven structures, I_{Fd} and I_{Fe} were found to have lower energies (the energies relative to I_{Fb} are −0.7 and −1.3 kcal/mol, respectively). These structures, in which the trifluoromethyl group is directed to the other side of the chloride ligand, avoid

https://doi.org/10.1021/acsomega.2c04645
ACS Omega 2022, 7, 36634−36642

Table 1. Relative Gibbs Free Energy $\Delta\Delta G^{333\,K}$ and Boltzmann Distribution for Lower-Energy Transition-State Structures

	TS_x[a]		TS_{Mx}		TS_{Fx}	
x	$\Delta\Delta G^{333\,K}$ (kcal/mol)	$\exp\left(-\frac{\Delta\Delta G^{333\,K}}{R\times 333\,K}\right)$[b]	$\Delta\Delta G^{333\,K}$ (kcal/mol)	$\exp\left(-\frac{\Delta\Delta G^{333\,K}}{R\times 333\,K}\right)$[b]	$\Delta\Delta G^{333\,K}$ (kcal/mol)	$\exp\left(-\frac{\Delta\Delta G^{333\,K}}{R\times 333\,K}\right)$[b]
B5dd	−0.03	1.049	0.0	1.000	2.4	0.025
A3dd	0.0	1.000	0.1	0.840	3.8	0.003
A2dd	0.5	0.506	3.1	0.010	3.0	0.010
A4dd	0.9	0.251	2.8	0.015	6.1	0.000
A5dd	1.6	0.087	2.0	0.052	4.9	0.001
A3du	1.9	0.060	3.6	0.004	9.0	0.000
B3dd	2.0	0.045	0.2	0.725	2.0	0.046
B4dd	4.2	0.002	0.5	0.465	0.0	1.000

[a] $\mathbf{TS_{Anyz}}$ and $\mathbf{TS_{Bnyz}}$ correspond to $\mathbf{TS_{rnyz}}$ and $\mathbf{TS_{snyz}}$, respectively, in ref 6. [b] R is the gas constant.

the repulsive interactions between the fluoride atoms in the trifluoromethyl group and the chloride ligand. In addition, the interactions of the fluoride atom with not only the hydrogen atoms of a pentamethylcyclopentadienyl ligand but also the hydrogen of the ethyl group in the other thiolate ligand were observed (Figure S2). The NCI plot also indicates the CF/π interaction[15] between a C−F bond and the terminal phenyl group of the thiolate ligand in $\mathbf{I_{Fe}}$. Thus, a trifluoromethyl group undergoes dispersion interactions with the C−H bond and phenyl group in the surrounding ligands.

These results show that methyl or trifluoromethyl substitution certainly affects the structures of ruthenium−allenylidene complexes, but the effects are relatively small from a free energy point of view. The energy differences between the obtained equilibrium structures are within 3.4 and 2.1 kcal/mol for **3b** ($\mathbf{I_{Ma}}$−$\mathbf{I_{Mf}}$) and **3c** ($\mathbf{I_{Fa}}$−$\mathbf{I_{Ff}}$), respectively (2.1 kcal/mol for **3a**). Thus, further examinations of the transition-state structures for the attack of nucleophiles are required to clarify the enantioselectivity in the catalytic substitution reaction.

Transition-State Structures. In our previous study,[6] we explored 56 transition-state structures for the attacks of the enol isomer on **3a** and found that the nucleophile attacks from the direction of the chloride ligand to either the A-face (*Si*-face) or the B-face (*Re*-face) of the allenylidene moiety. In the A-face attack, two conformations of the terminal phenyl group in the thiolate ligand are possible, while only one conformation leads to the B-face attack. We concluded that the difference leads to the preferential formation of the *R*-product (**(*R*)4a**) over the *S*-product (**(*S*)4a**) in terms of probability distributions (enantiomeric excess was calculated to be 27% ee).

As in the case with **3a**, we investigated 56 transition-state structures for attacks of enol to **3b** ($\mathbf{TS_{MAnyz}}$ and $\mathbf{TS_{MBnyz}}$, in which enol attacks from A- and B-faces, respectively (n = 1−7; y, z = d or u (showing the direction of the ethyl group in thiolate ligands)); Figures S4−S7). Among the calculated transition-state structures, $\mathbf{TS_{MB5dd}}$, which corresponds to the B-face attack, has the lowest Gibbs free energy at 333 K (Figure 2). The other transition states corresponding to the B-face attack, $\mathbf{TS_{MB3dd}}$ and $\mathbf{TS_{MB4dd}}$, have almost the same free energies (the free energies relative to $\mathbf{TS_{MB5dd}}$, $\Delta\Delta G^{333\,K}$, are 0.2 and 0.5 kcal/mol, respectively.) In contrast, the energies of the transition states where enol attacks from the A-face, $\mathbf{TS_{MA2dd}}$ and $\mathbf{TS_{MA4dd}}$, are slightly higher in free energies than $\mathbf{TS_{MB5dd}}$ ($\Delta\Delta G^{333\,K}$ are 3.1 and 2.8 kcal/mol, respectively), although $\mathbf{TS_{MA3dd}}$ has almost the same free energy ($\Delta\Delta G^{333\,K}$ = 0.1 kcal/mol).

The obtained results indicate that the effect of the methyl group in the transition-state structures for the A-face attack is different from that in the structures for the B-face attack. In the transition states for the A-face attack, the methyl group of the allenylidene ligand faces the terminal phenyl group of the thiolate ligand. The structures with conformation H at the terminal phenyl group of the thiolate ligand (Figure 2), $\mathbf{TS_{MA2dd}}$ and $\mathbf{TS_{MA4dd}}$, are sterically more inconvenient than the structures with conformation V, $\mathbf{TS_{MA3dd}}$ and $\mathbf{TS_{MA5dd}}$, which increases their relative free energies. In contrast, the steric repulsions caused by the methyl group are relatively smaller in the transition states for the B-face attack because the methyl group is directed in the opposite direction of the terminal phenyl group of the thiolate ligand. Moreover, the dispersion interactions between the phenyl group in the allenylidene and the terminal phenyl group of the thiolate ligand increase slightly upon the introduction of the methyl group. Thus, the methyl moiety located away from the terminal phenyl group of the thiolate ligand lowers the relative energies of these structures compared with those in the transition states corresponding to the A-face attack (Table 1).

Among the transition-state structures with lower free energies, the structures that provide the *S*-product (**(*S*)4b**) through the B-face attack ($\mathbf{TS_{MB5dd}}$, $\mathbf{TS_{MB3dd}}$, and $\mathbf{TS_{MB4dd}}$) are larger in number than those providing the *R*-product (**(*R*)4b**) through the A-face attack ($\mathbf{TS_{MA3dd}}$). Thus, **(*S*)4b** is preferentially formed over **(*R*)4b** based on the probability distributions (Table 1), and the enantiomeric excess is estimated to be 40% ee. This result is in contrast with our previous results that the number of lower-energy structures leading to the *R*-product (**(*R*)4a**) is larger than that of the structures leading to the *S*-product (**(*S*)4a**) in the case of the reaction of **3a**. This result suggests that the substitution of a methyl group for a propargylic hydrogen atom in propargylic alcohol makes the stereoselectivity inverse.

We further calculated transition-state structures for the attack of enol to **3c** ($\mathbf{TS_{FAnyz}}$ for structures giving the *S*-product through the A-face attack and $\mathbf{TS_{MBnyz}}$ for structures giving the *R*-product through the B-face attack; Figures S4, S8, S9, and S10). Among the structures, $\mathbf{TS_{FB4dd}}$ has the lowest free energy, and the structure having the second lowest energy, $\mathbf{TS_{FB3dd}}$, is higher in energy than $\mathbf{TS_{FB4dd}}$ by 2.0 kcal/mol (Table 1). Compared to the corresponding transition states $\mathbf{TS_{B4dd}}$[16] and $\mathbf{TS_{MB4dd}}$, the location of enol in $\mathbf{TS_{FB4dd}}$ slips slightly from the direction of the chloride ligand to that of the other terminal phenyl group in the thiolate ligand, and the fluoride atom at the trifluoromethyl group interacts with the C(sp^2)−H bond of the terminal phenyl group in the thiolate

https://doi.org/10.1021/acsomega.2c04645
ACS Omega 2022, 7, 36634−36642

ligand (the distances between the hydrogen atom and the fluoride atom are 2.66 and 2.71 Å, respectively, shown in Figure 3a). The other fluoride atom also interacts with not

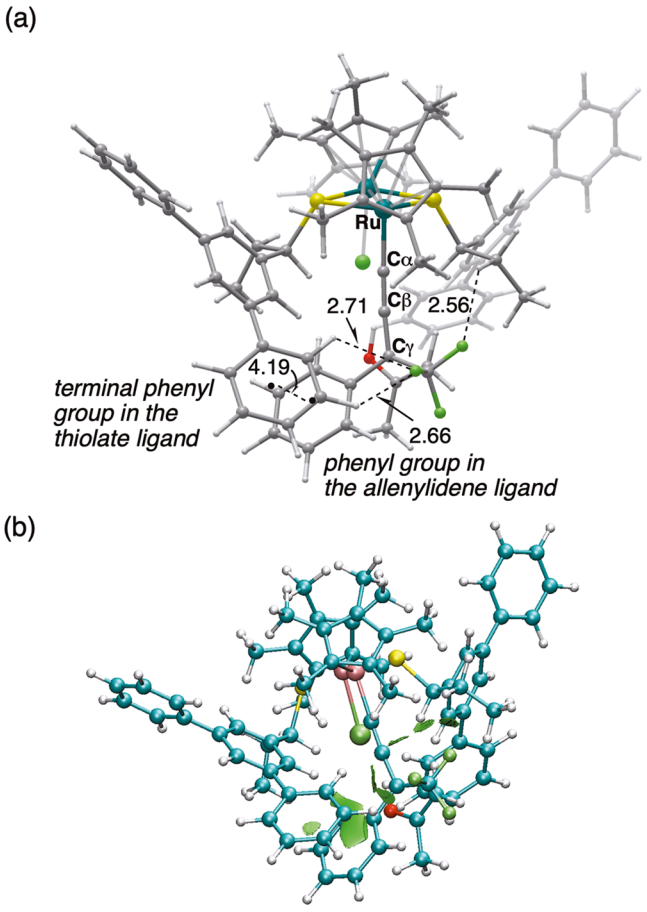

Figure 3. (a) Transition-state structure $\mathbf{TS}_{\mathbf{FB4dd}}$. The distances are given in Å. (b) NCI plot around the terminal phenyl group in $\mathbf{TS}_{\mathbf{FB4dd}}$. Green surfaces show van der Waals interactions.

only the hydrogen atom of the ethyl group at the other thiolate ligand (the distance between the hydrogen atom and the fluoride atom is 2.56 Å) but also the hydrogen atoms of the pentamethylcyclopentadienyl ligand (the distance between the hydrogen atoms and the fluoride atom is 2.75 and 2.79 Å. These interactions and the $\pi-\pi$ interactions lower the free energy of the transition state compared to those of other structures (Figure 3b for NCI plot). As a result, the B-face attack leading to the *R*-product ((***R***)**4c**) is favorable compared to the A-face attack leading to the *S*-product ((***S***)**4c**), as is the case for the attack of enol on **3b**, and the enantiomeric excess was estimated to increase (97% ee). This result indicates that replacing the methyl group at the propargylic position with a trifluoromethyl group leads to a higher enantioselectivity. This result is consistent with the recent experimental results of asymmetric propargylic phosphinylation reactions between propargylic alcohol bearing a trifluoromethyl group at the propargylic position and diphenylphosphine oxide catalyzed by **1a** or **1b**, where phosphorous acid, a tautomer of phosphine oxide, has been supposed to be a nucleophile (Scheme 4).[7] The computational and experimental results suggest that not the nucleophile but the substituent at the propargylic position of propargylic alcohols controls the enantioselectivity of diruthenium-catalyzed propargylic substitution reactions.

Effects of Substituents on Reactivities. Finally, we examined the effects of substituents on the electrophilicity of the C_γ atom in ruthenium−allenylidene complexes **3b** and **3c**. In the reaction of **3a**, the energy of $\mathbf{TS}_{\mathbf{A3dd}}$[17] relative to (**Ib** + acetone), $\Delta G^{333\,K}$, was reported to be 26.7 kcal/mol (Figure 4a).[6] The corresponding relative energies of $\mathbf{TS}_{\mathbf{MB5dd}}$ and $\mathbf{TS}_{\mathbf{FB4dd}}$ were 35.5 and 31.5 kcal/mol, respectively, which are much higher than that of $\mathbf{TS}_{\mathbf{A3dd}}$ (Figure 4b,c).[18] Although the LUMO of $\mathbf{I}_{\mathbf{Fe}}$ had the lowest energy level among three ruthenium−allenylidene complexes (−3.93, −3.80, and −4.21 eV for $\mathbf{I}_{\mathbf{b}}$, $\mathbf{I}_{\mathbf{Mb}}$, and $\mathbf{I}_{\mathbf{Fe}}$, respectively; Figure 5), the population of the C_γ atom in the LUMO of $\mathbf{I}_{\mathbf{Fe}}$ was the smallest because of the polarization of π-orbitals in the allenylidene moiety caused by the electronegative trifluoromethyl group (0.320, 0.322 and 0.290 for $\mathbf{I}_{\mathbf{b}}$, $\mathbf{I}_{\mathbf{Mb}}$, and $\mathbf{I}_{\mathbf{Fe}}$, respectively).[19] These two factors determine the order in electrophilicity of the C_γ atom.[20]

CONCLUSIONS

Based on our previous research on the transition-state model for the asymmetric propargylic substitution reactions catalyzed by optically active thiolate-bridged diruthenium complexes, we examined the effects of propargylic substituent (methyl or trifluoromethyl group) on both the enantioselectivity and reactivity of the reactions via ωB97X-D-level DFT calculations. Calculations showed that methyl or trifluoromethyl substitution affected the structures of ruthenium−allenylidene complexes, but the effects were found to be relatively small from a free energy point of view. Thus, transition-state structures for the attack of nucleophiles were explored. In the case of propargylic alcohol bearing a methyl group at the propargylic position, the number of lower-energy structures through the B-face attack was larger than that of the structures through the A-face attack. This result contrasts with the results of our previous work, which studied reactions of a propargylic alcohol without a methyl group, indicating that the methyl group substitution at the propargylic position reverses the enantioselectivity. In the case of trifluoromethyl group substitution, the specific transition-state structure for the B-face attack was found to be much lower in free energy than other structures because of the interactions of fluorine atoms with C−H bonds of other ligands. The evidence suggested that the substitution of a trifluoromethyl group for a methyl group at the propargylic position results in higher enantioselectivity. However, methyl or trifluoromethyl substitution was found to make the electrophilicity of the C_γ atom in ruthenium−allenylidene complexes lower.

COMPUTATIONAL DETAILS

DFT calculations were carried out with the Gaussian 09[22] program package. Geometry optimization and analytical vibrational frequency analysis were performed via the restricted Kohn−Sham DFT using the long-range corrected (LC) hybrid density functional with empirical dispersion corrections (ωB97X-D).[23,24] In the numerical integration, a larger grid (*superfinegrid*) was used.[22] Pople's 6-31G(d) basis set was used for the H, C, N, O, F, S, and Cl atoms,[25] and the SDD basis set with the effective core potential was used for the Ru atom[26] for the Gaussian basis functions (6d type polarization functions). The solvent effects of acetone were estimated by the polarizable continuum model with integral equation formalism (IEF-PCM)[27] for the gas-phase optimized structures. For the IEF-PCM calculations, the SDD basis set was used for the Ru

https://doi.org/10.1021/acsomega.2c04645
ACS Omega 2022, 7, 36634−36642

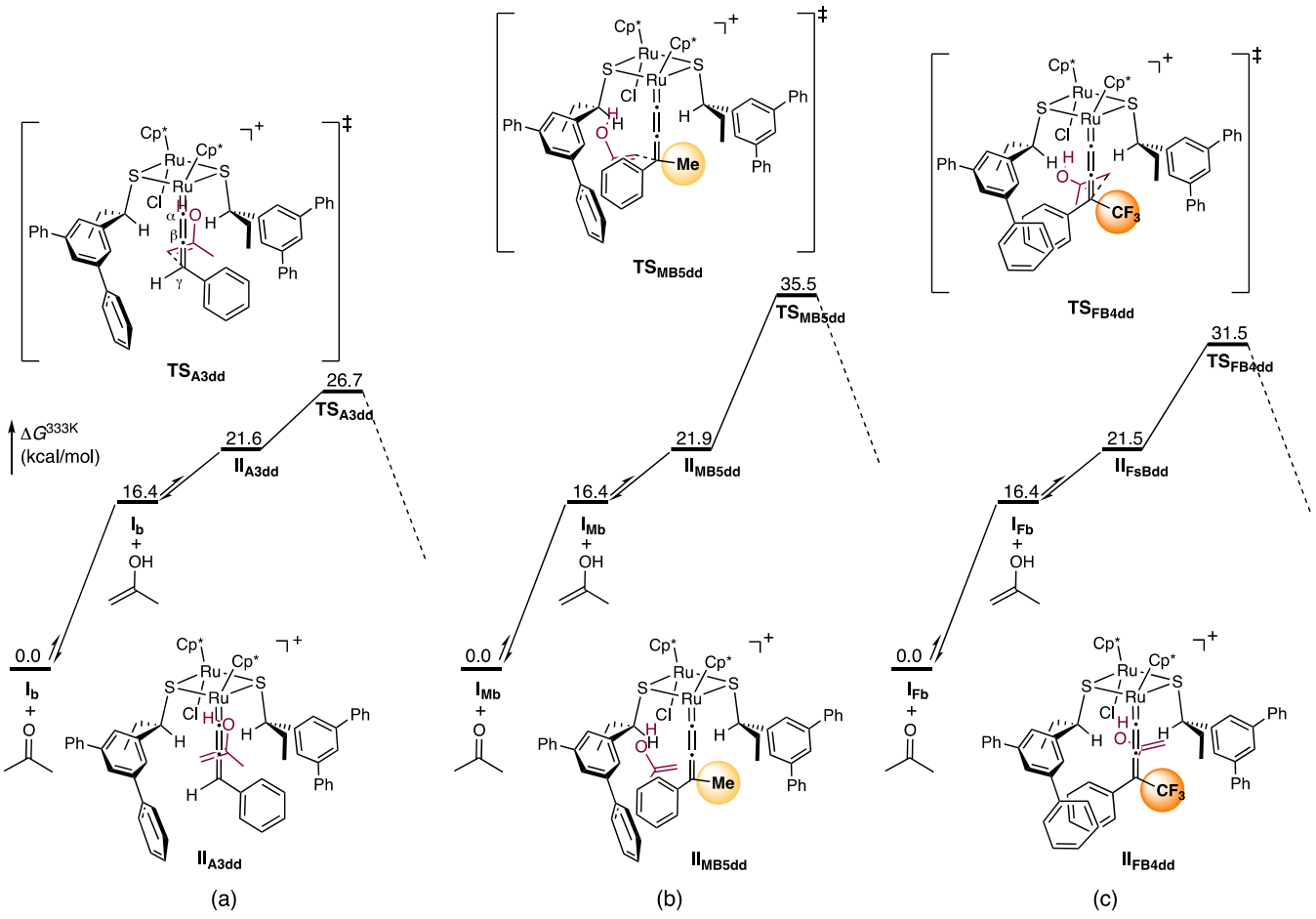

Figure 4. Relative Gibbs free energy diagrams, $\Delta G^{333\,K}$, for the reaction pathways via (a) $\mathbf{TS}_{A3dd}$, (b) $\mathbf{TS}_{MB5dd}$, and (c) $\mathbf{TS}_{FB4dd}$ at the ωB97X-D(IEF-PCM)/(SDD,6-311++G(*d*,*p*))//ωB97X-D/(SDD,6-31G(d)) level of theory (kcal/mol). Reaction pathway (a) was reported in ref 6.[17]

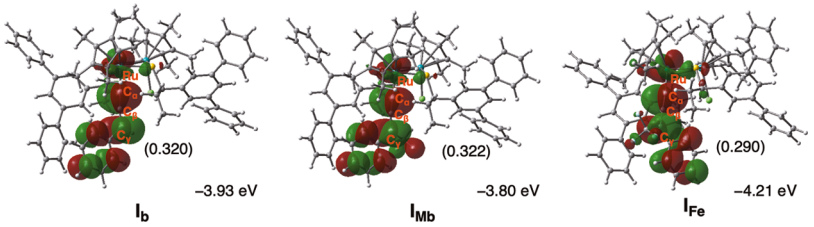

Figure 5. LUMOs of ruthenium−allenylidene complexes $\mathbf{I}_b$, $\mathbf{I}_{Mb}$, and $\mathbf{I}_{Fe}$. The population of the C_γ atom in the LUMO is shown in parentheses.

atom and the 6-311++G(d,p) basis set (5d-type polarization functions) was used for other atoms. The Gibbs free energy at 333 K was estimated by the IEF-PCM energy and the gas-phase thermal value (ωB97X-D(IEF-PCM)/(SDD,6-311++G-(d,p))//ωB97X-D/(SDD,6-31G(d))). The method used in the present study was the same as that used in our previous study.[6]

■ ASSOCIATED CONTENT

Supporting Information

The Supporting Information is available free of charge at https://pubs.acs.org/doi/10.1021/acsomega.2c04645.

Tables listing the energies and geometries and figures containing structures (PDF)

■ AUTHOR INFORMATION

Corresponding Author

Ken Sakata − *Faculty of Pharmaceutical Sciences, Toho University, Funabashi, Chiba 274-8510, Japan;* orcid.org/0000-0002-6920-0735; Email: ken.sakata@phar.toho-u.ac.jp

Authors

Yuuri Uehara − *Faculty of Pharmaceutical Sciences, Toho University, Funabashi, Chiba 274-8510, Japan*

Shiona Kohara − *Faculty of Pharmaceutical Sciences, Toho University, Funabashi, Chiba 274-8510, Japan*

Takeshi Yoshikawa − *Faculty of Pharmaceutical Sciences, Toho University, Funabashi, Chiba 274-8510, Japan;* orcid.org/0000-0002-7489-5252

https://doi.org/10.1021/acsomega.2c04645
ACS Omega 2022, 7, 36634−36642

Yoshiaki Nishibayashi − *Department of Applied Chemistry, School of Engineering, The University of Tokyo, Tokyo 113-8656, Japan;* orcid.org/0000-0001-9739-9588

Complete contact information is available at: https://pubs.acs.org/10.1021/acsomega.2c04645

Notes

The authors declare no competing financial interest.

■ ACKNOWLEDGMENTS

This work was supported by Grants-in-Aid for Scientific Research (Nos. JP20H05671 and 20K05532) from JSPS. The computation was performed using the Research Center for Computational Science, Okazaki, Japan (Project: 22-IMS-C053).

■ REFERENCES

(1) (a) Nishibayashi, Y. Development of asymmetric propargylic substitution reactions using transition metal catalysts. *Chem. Lett.* **2021**, *50*, 1282−1288. (b) Tsuji, H.; Kawatsura, M. Transition-metal-catalyzed propargylic substitution of propargylic alcohol derivatives bearing an internal alkyne group. *Asian J. Org. Chem.* **2020**, *9*, 1924−1941. (c) Zhang, D.-Y.; Hu, X.-P. Recent advances in copper-catalyzed propargylic substitution. *Tetrahedron Lett.* **2015**, *56*, 283−295. (d) Nishibayashi, Y. Transition-metal-catalyzed enantioselective propargylic substitution reactions of propargylic alcohol derivatives with nucleophiles. *Synthesis* **2012**, *2012*, 489−503. (e) Ding, C.-H.; Hou, X.-L. Catalytic asymmetric propargylation. *Chem. Rev.* **2011**, *111*, 1914−1937. (f) Detz, R. J.; Hiemstra, H.; van Maarseveen, J. H. Catalyzed propargylic substitution. *Eur. J. Org. Chem.* **2009**, *2009*, 6263−6276. (g) Ljungdahl, N.; Kann, N. Transition-metal-catalyzed propargylic substitution. *Angew. Chem., Int. Ed.* **2009**, *48*, 642−644.

(2) Inada, Y.; Nishibayashi, Y.; Uemura, S. Ruthenium-catalyzed asymmetric propargylic substitution reactions of propargylic alcohols with acetone. *Angew. Chem., Int. Ed.* **2005**, *44*, 7715−7717.

(3) (a) Matsuzawa, H.; Miyake, Y.; Nishibayashi, Y. Ruthenium-catalyzed enantioselective propargylation of aromatic compounds with propargylic alcohols via allenylidene intermediates. *Angew. Chem., Int. Ed.* **2007**, *46*, 6488−6491. (b) Smith, S. W.; Fu, G. C. Nickel-catalyzed asymmetric cross-couplings of racemic propargylic halides with arylzinc reagents. *J. Am. Chem. Soc.* **2008**, *130*, 12645−12647. (c) Fukamizu, K.; Miyake, Y.; Nishibayashi, Y. Ruthenium-catalyzed enantioselective carbon−carbon bond forming reaction via allenylidene-ene process: synthetic approach to chiral heterocycles such as chromane, thiochromane, and 1,2,3,4-tetrahydroquinoline derivatives. *J. Am. Chem. Soc.* **2008**, *130*, 10498−10499. (d) Detz, R. J.; Delville, M. M. E.; Hiemstra, H.; van Maarseveen, J. H. Enantioselective copper-catalyzed propargylic amination. *Angew. Chem., Int. Ed.* **2008**, *47*, 3777−3780. (e) Hattori, G.; Matsuzawa, H.; Miyake, Y.; Nishibayashi, Y. Copper-catalyzed asymmetric propargylic substitution reactions of propargylic acetates with amines. *Angew. Chem., Int. Ed.* **2008**, *47*, 3781−3783. (f) Fang, P.; Hou, X.-L. Asymmetric copper-catalyzed propargylic substitution reaction of propargylic acetates with enamines. *Org. Lett.* **2009**, *11*, 4612−4615. (g) Hattori, G.; Yoshida, A.; Miyake, Y.; Nishibayashi, Y. Enantioselective ring-opening reactions of racemic ethynyl epoxides via copper-allenylidene intermediates: efficient approach to chiral *β*-amino alcohols. *J. Org. Chem.* **2009**, *74*, 7603−7607. (h) Kanao, K.; Miyake, Y.; Nishibayashi, Y. Ruthenium-catalyzed enantioselective [3+3] cycloaddition of propargylic alcohols with 2-naphthols. *Organometallics* **2010**, *29*, 2126−2131. (i) Hattori, G.; Sakata, K.; Matsuzawa, H.; Tanabe, Y.; Miyake, Y.; Nishibayashi, Y. Copper-catalyzed enantioselective propargylic amination of propargylic esters with amines: copper-allenylidene complexes as key intermediates. *J. Am. Chem. Soc.* **2010**, *132*, 10592−10608. (j) Detz, R. J.; Abiri, Z.; le Griel, R.; Hiemstra, H.; van Maarseveen, J. H. Enantioselective copper-catalysed propargylic substitution: Synthetic scope study and application in formal total syntheses of (+)-anisomycin and (−)-cytoxazone. *Chem. − Eur. J.* **2011**, *17*, 5921−5930. (k) Zhang, C.; Wang, Y.-H.; Hu, X.-H.; Zheng, Z.; Xu, J.; Hu, X.-P. Chiral tridentate P,N,N ligands for highly enantioselective copper-catalyzed propargylic amination with both primary and secondary amines as nucleophiles. *Adv. Synth. Catal.* **2012**, *354*, 2854−2858. (l) Zhu, F.-L.; Zou, Y.; Zhang, D.-Y.; Wang, Y.-H.; Hu, X.-H.; Chen, S.; Xu, J.; Hu, X.-P. Enantioselective copper-catalyzed decarboxylative propargylic alkylation of propargyl *β*-ketoesters with a chiral ketimine P,N,N-ligand. *Angew. Chem., Int. Ed.* **2014**, *53*, 1410−1414. (m) Nakajima, K.; Shibata, M.; Nishibayashi, Y. Copper-catalyzed enantioselective propargylic etherification of propargylic esters with alcohols. *J. Am. Chem. Soc.* **2015**, *137*, 2472−2475. (n) Zhang, D.-Y.; Shao, L.; Xu, J.; Hu, X.-P. Copper-catalyzed asymmetric formal [3 + 2] cycloaddition of propargylic acetates with hydrazines: enantioselective synthesis of optically active 2-pyrazolines. *ACS Catal.* **2015**, *5*, 5026−5030. (o) Wang, Q.; Li, T.-R.; Lu, L.-Q.; Li, M.-M.; Zhang, K.; Xiao, W.-J. Catalytic asymmetric [4 + 1] annulation of sulfur ylides with copper−allenylidene intermediates. *J. Am. Chem. Soc.* **2016**, *138*, 8360−8363. (p) Guisán-Ceinos, M.; Martín- Heras, V.; Tortosa, M. Regio- and stereospecific copper-catalyzed substitution reaction of propargylic ammonium salts with aryl Grignard reagents. *J. Am. Chem. Soc.* **2017**, *139*, 8448−8451. (q) Cheng, L.-J.; Brown, A. P. N.; Cordier, C. J. Enantioselective propargylic [1,3]-rearrangements: copper-catalyzed *O*-to-*N* migrations toward C−N bond formation. *Chem. Sci.* **2017**, *8*, 4299−4305. (r) Li, R.-Z.; Tang, H.; Yang, K. R.; Wan, L.-Q.; Zhang, X.; Liu, J.; Fu, Z.; Niu, D. Enantioselective propargylation of polyols and desymmetrization of *meso* 1,2-diols by copper/borinic acid dual catalysis. *Angew. Chem., Int. Ed.* **2017**, *56*, 7213−7217. (s) Li, R.-Z.; Tang, H.; Wan, L.; Zhang, X.; Fu, Z.; Liu, J.; Yang, S.; Jia, D.; Niu, D. Site-divergent delivery of terminal propargyls to carbohydrates by synergistic catalysis. *Chem* **2017**, *3*, 834−845. (t) Zhang, K.; Lu, L.-Q.; Yao, S.; Chen, J.-R.; Shi, D.-Q.; Xiao, W.-J. Enantioconvergent copper catalysis: *in situ* generation of the chiral phosphorus ylide and its Wittig reactions. *J. Am. Chem. Soc.* **2017**, *139*, 12847−12854. (u) Xu, H.; Laraia, L.; Schneider, L.; Louven, K.; Strohmann, C.; Antonchick, A. P.; Waldmann, H. Highly enantioselective catalytic vinylogous propargylation of coumarins yields a class of autophagy inhibitors. *Angew. Chem., Int. Ed.* **2017**, *56*, 11232−11236. (v) Gómez, J. E.; Guo, W.; Gaspa, S.; Kleij, W. Copper-catalyzed synthesis of *γ*-amino acids featuring quaternary stereocenters. *Angew. Chem., Int. Ed.* **2017**, *56*, 15035−15038. (w) Shemet, A.; Carreira, E. M. Total synthesis of (−)-rhazinilam and formal synthesis of (+)-eburenine and (+)-aspidospermidine: asymmetric Cu-catalyzed propargylic substitution. *Org. Lett.* **2017**, *19*, 5529−5532.

(4) (a) Ota, Y.; Kondoh, A.; Terada, M. Enantioselective intramolecular Nicholas reaction catalyzed by chiral phosphoric acid: enantioconvergent synthesis of seven-membered cyclic ethers from racemic diols. *Angew. Chem., Int. Ed.* **2018**, *57*, 13917−13921. (b) Fu, Z.; Deng, N.; Su, S.-N.; Li, H.; Li, R.-Z.; X Zhang, X.; Liu, J.; Niu, D. Diastereo- and enantioselective propargylation of 5H-thiazol-4-ones and 5H-oxazol-4-ones as enabled by Cu/Zn and Cu/Ti catalysis. *Angew. Chem., Int. Ed.* **2018**, *57*, 15217−15221. (c) Watanabe, K.; Miyazaki, Y.; Okubo, M.; Zhou, B.; Tsuji, H.; Kawatsura, M. Nickel-catalyzed asymmetric propargylic amination of propargylic carbonates bearing an internal alkyne group. *Org. Lett.* **2018**, *20*, 5448−5451. (d) Gómez, J. E.; Cristòfol, À.; Kleij, A. W. Copper-catalyzed enantioselective construction of tertiary propargylic sulfones. *Angew. Chem., Int. Ed.* **2019**, *58*, 3903−3907. (e) Lu, F.-D.; Liu, D.; Zhu, L.; Lu, L.-Q.; Yang, Q.; Zhou, Q.-Q.; Wei, Y.; Lan, Y.; Xiao, W.-J. Asymmetric propargylic radical cyanation enabled by dual organophotoredox and copper catalysis. *J. Am. Chem. Soc.* **2019**, *141*, 6167−6172. (f) Zhang, Z.-J.; Zhang, L.; Geng, R.-L.; Song, J.; Chen, X.-H.; Gong, L.-Z. N-Heterocyclic carbene/copper cooperative catalysis for the asymmetric synthesis of spirooxindoles. *Angew. Chem., Int. Ed.* **2019**, *58*, 12190−12194. (g) Gao, X.; Cheng, R.; Xiao, Y.-L.; Wan, X.-L.; Zhang, X. Copper-catalyzed highly enantioselective difluoroalkylation of secondary propargyl sulfonates with difluoroenoxysilanes. *Chem* **2019**, *5*, 2987−2999. (h) Liu, S.; Nakajima, K.;

Nishibayashi, Y. Copper-catalysed enantioselective intramolecular etherification of propargylic esters: synthetic approach to chiral isochromans. *RSC Adv.* **2019**, *9*, 18918−18922. (i) Peng, L.; He, Z.; Xu, X.; Guo, C. Cooperative Ni/Cu-catalyzed asymmetric propargylic alkylation of aldimine esters. *Angew. Chem., Int. Ed.* **2020**, *59*, 14270−14274. (j) Li, R.-Z.; Liu, D.-Q.; Niu, D. Asymmetric *O*-propargylation of secondary aliphatic alcohols. *Nat. Catal.* **2020**, *3*, 672−680. (k) Huo, H.; Gorsline, B. J.; Fu, G. C. Catalyst-controlled doubly enantioconvergent coupling of racemic alkyl nucleophiles and electrophiles. *Science* **2020**, *367*, 559−564. (l) Chang, X.; Zhang, J.; Peng, L.; Guo, C. Collective synthesis of acetylenic pharmaceuticals via enantioselective Nickel/Lewis acid-catalyzed propargylic alkylation. *Nat. Commun.* **2021**, *12*, No. 299. (m) Tsuji, H.; Shimizu, Y.; Miyazaki, Y.; Kawatsura, M. Nickel-catalyzed asymmetric propargylic amination of propargylic carbonates with aniline derivatives. *Chem. Lett.* **2021**, *50*, 1002−1005.

(5) (a) Saha, S.; Schneider, C. Directing group assisted nucleophilic substitution of propargylic alcohols via *o*-quinone methide intermediates: Brønsted acid catalyzed, highly enantio- and diastereoselective synthesis of 7-alkynyl-12a-acetamido-substituted benzoxanthenes. *Org. Lett.* **2015**, *17*, 648−651. (b) Chen, M.; Sun, J. How understanding the role of an additive can lead to an improved synthetic protocol without an additive: organocatalytic synthesis of chiral diarylmethyl alkynes. *Angew. Chem., Int. Ed.* **2017**, *56*, 11966−11970. (c) Wendlandt, A. E.; Vangal, P.; Jacobsen, E. N. Quaternary stereocentres via an enantioconvergent catalytic S_N1 reaction. *Nature* **2018**, *556*, 447−451. (d) Bai, J.-F.; Yasumoto, K.; Kano, T.; Maruoka, K. Asymmetric synthesis of chiral 1,4-enynes through organocatalytic alkenylation of propargyl alcohols with trialkenylboroxines. *Angew. Chem., Int. Ed.* **2019**, *58*, 8898−8901. (e) Kikuchi, J.; Takano, K.; Ota, Y.; Umemiya, S.; Terada, M. Chiral Brønsted acid catalyzed enantioconvergent propargylic substitution reaction of racemic secondary propargylic alcohols with thiols. *Chem. − Eur. J.* **2020**, *26*, 11124−11128. (f) Ma, Y.; Liu, X.; Mao, Y.; Huang, J.; Ma, S.; Liu, L. Redox deracemization of diarylmethyl alkynes. *Org. Chem. Front.* **2020**, *7*, 2526−2530. (g) Li, F.; Chen, X.; Liang, S.; Shi, Z.; Li, P.; Li, W. Organocatalytic site- and stereoselective 1,6-additions of *N*-aryl-3-oxobutanamides to propargylic aza-*p*-quinone methides. *Org. Chem. Front.* **2020**, *7*, 3446−3451.

(6) Sakata, K.; Goto, Y.; Yoshikawa, T.; Nishibayashi, Y. Enantioselectivity in ruthenium-catalyzed propargylic substitution reactions of propargylic alcohols with acetone: a DFT study. *Chem. − Asian J.* **2021**, *16*, 3760−3766.

(7) Liu, S.; Tanabe, S.; Kuriyama, S.; Sakata, K.; Nishibayashi, Y. Ruthenium-catalyzed enantioselective propargylic phosphinylation of propargylic alcohols with phosphine oxides. *Angew. Chem., Int. Ed.* **2021**, *60*, 11231−11236.

(8) Sakata, K.; Miyake, Y.; Nishibayashi, Y. A DFT study on the reaction pathways for carbon−carbon bond-forming reactions between propargylic alcohols and alkenes or ketones catalyzed by thiolate-bridged diruthenium complexes. *Chem. − Asian J.* **2009**, *4*, 81−88.

(9) (a) Nishibayashi, Y.; Milton, M. D.; Inada, Y.; Yoshikawa, M.; Wakiji, I.; Hidai, M.; Uemura, S. Ruthenium-catalyzed propargylic substitution reactions of propargylic alcohols with oxygen-, nitrogen-, and phosphorus-centered nucleophiles. *Chem. − Eur. J.* **2005**, *11*, 1433−1451. (b) Miyake, Y.; Uemura, S.; Nishibayashi, Y. Catalytic propargylic substitution reactions. *ChemCatChem* **2009**, *1*, 342−356.

(10) (a) Ammal, S. C.; Yoshikai, N.; Inada, Y.; Nishibayashi, Y.; Nakamura, E. Synergistic dimetallic effects in propargylic substitution reaction catalyzed by thiolate-bridged diruthenium complex. *J. Am. Chem. Soc.* **2005**, *127*, 9428−9438. (b) Sakata, K.; Nishibayashi, Y. Mechanism and reactivity of catalytic propargylic substitution reactions via metal−allenylidene intermediates: a theoretical perspective. *Catal. Sci. Technol.* **2018**, *8*, 12−25.

(11) (a) Contreras-García, J.; Johnson, E. R.; Keinan, S.; Chaudret, R.; Piquemal, J.-P.; Beratan, D. N.; Yang, W. NCIPLOT: a program for plotting noncovalent interaction regions. *J. Chem. Theory Comput.* **2011**, *7*, 625−632. (b) Boto, R. A.; Peccati, F.; Laplaza, R.; Quan, C.; Carbone, A.; Piquemal, J.-P.; Maday, Y.; Contreras-García, J. NCIPLOT4: fast, robust, and quantitative analysis of noncovalent interactions. *J. Chem. Theory Comput.* **2020**, *16*, 4150−4158.

(12) The examination for the model substitution reaction of the hydrogen atom for the terminal phenyl group of the thiolate ligand in the ruthenium-allenylidene complex fixed with the structures indicates that the interactions between the allenylidene complex and the terminal phenyl group of the thiolate ligand in $\mathbf{I}_{Ma}$ and $\mathbf{I}_{Mb}$ are slightly larger than those in $\mathbf{I}_a$ and $\mathbf{I}_b$, respectively. See Figure S3.

(13) For the complexation energy which consists of two energy terms, the destabilization caused by the deformation of two fragments (DEF), i.e., the cationic diruthenium complex and allenylidene ligand, and the stabilization by the interaction between the two fragments (INT), see Table S3.

(14) In $\mathbf{I}_{Fb}$ and $\mathbf{I}_{Fb'}$, the trifluoromethyl group is directed to the chloride ligand. Thus, the trifluoromethyl group intends to keep away from the chloride ligand. The direction away from the chloride ligand in $\mathbf{I}_{Fb}$ is different from that in $\mathbf{I}_{Fb'}$.

(15) (a) Kawahara, S.-i.; Tsuzuki, S.; Uchimaru, T. Theoretical study of the C−F/π interaction: attractive interaction between fluorinated alkane and an electron-deficient π-system. *J. Phys. Chem. A* **2004**, *108*, 6744−6749. (b) Ams, M. R.; Fields, M.; Grabnic, T.; Janesko, B. G.; Zeller, M.; Sheridan, R.; Shay, A. Unraveling the role of alkyl F on CH−π interactions and uncovering the tipping point for fluorophobicity. *J. Org. Chem.* **2015**, *80*, 7764−7769.

(16) $\mathbf{TS}_{B4dd}$ corresponds to $\mathbf{TS}_{s4dd}$ in ref 6.

(17) $\mathbf{TS}_{A3dd}$ corresponds to $\mathbf{TS}_{r3dd}$ in ref 6.

(18) Propargylic alcohol bearing a methyl or trifluoromethyl group did not experimentally react in the reaction system.

(19) Trifluoromethyl group pulls the π-occupied orbitals in the allenylidene moiety to the C_γ atom. Thus, the amplitude of the C_γ atom in the π-unoccupied orbitals decreases.

(20) We applied the 2pπ orbital at the C_γ atom to the reference orbital, δ_r, and projected then this reference orbital onto the unoccupied orbital space of $\mathbf{I}_b$, $\mathbf{I}_{Mb}$, and $\mathbf{I}_{Fe}$ (here, 2pπ orbital is obtained by the LUMO of CH_3^+ which has the energy of −10.66 eV). The orbital has the energy expectation value, $\lambda_{unoc}(\delta_r)$, of −1.24, −0.91, and −1.06 eV for $\mathbf{I}_b$, $\mathbf{I}_{Mb}$, and $\mathbf{I}_{Fe}$, respectively, indicating that the electron-accepting ability at the C_γ atom increases in the order $\mathbf{I}_b > \mathbf{I}_{Fe} > \mathbf{I}_{Mb}$. See ref 21.

(21) (a) Sakata, K.; Fujimoto, H. Quantum chemical study of Lewis acid catalyzed allylboration of aldehydes. *J. Am. Chem. Soc.* **2008**, *130*, 12519−12526. (b) Fujimoto, H.; Sakata, K.; Fukui, K. Transient bonds and chemical reactivity of molecules. *Int. J. Quantum Chem.* **1996**, *60*, 401−408.

(22) Frisch, M. J.; Trucks, G. W.; Schlegel, H. B.; Scuseria, G. E.; Robb, M. A.; Cheeseman, J. R.; Scalmani, G.; Barone, V.; Mennucci, B.; Petersson, G. A.; Nakatsuji, H.; Caricato, M.; Li, X.; Hratchian, H. P.; Izmaylov, A. F.; Bloino, J.; Zheng, G.; Sonnenberg, J. L.; Hada, M.; Ehara, M.; Toyota, K.; Fukuda, R.; Hasegawa, J.; Ishida, M.; Nakajima, T.; Honda, Y.; Kitao, O.; Nakai, H.; Vreven, T.; Montgomery, J. A., Jr.; Peralta, J. E.; Ogliaro, F.; Bearpark, M.; Heyd, J. J.; Brothers, E.; Kudin, K. N.; Staroverov, V. N.; Kobayashi, R.; Normand, J.; Raghavachari, K.; Rendell, A.; Burant, J. C.; Iyengar, S. S.; Tomasi, J.; Cossi, M.; Rega, N.; Millam, J. M.; Klene, M.; Knox, J. E.; Cross, J. B.; Bakken, V.; Adamo, C.; Jaramillo, J.; Gomperts, R.; Stratmann, R. E.; Yazyev, O.; Austin, A. J.; Cammi, R.; Pomelli, C.; Ochterski, J. W.; Martin, R. L.; Morokuma, K.; Zakrzewski, V. G.; Voth, G. A.; Salvador, P.; Dannenberg, J. J.; Dapprich, S.; Daniels, A. D.; Farkas, Ö.; Foresman, J. B.; Ortiz, J. V.; Cioslowski, J.; Fox, D. J. *Gaussian 09*, revision D.01; Gaussian, Inc.: Wallingford, CT, 2009.

(23) Chai, J.-D.; Head-Gordon, M. Long-range corrected hybrid density functionals with damped atom−atom dispersion corrections. *Phys. Chem. Chem. Phys.* **2008**, *10*, 6615−6620.

(24) For the assessment of ωB97X-D functional for organometallic compounds, see: Raju, R. K.; Bengali, A. A.; Brothers, E. N. A unified set of experimental organometallic data used to evaluate modern theoretical methods. *Dalton Trans.* **2016**, *45*, 13766−13778.

https://doi.org/10.1021/acsomega.2c04645
ACS Omega 2022, 7, 36634−36642

(25) Hehre, W. J.; Radom, L.; Schleyer, P. R.; Pople, J. A. *Ab Initio Molecular Orbital Theory*; Wiley: New York, 1986.
(26) Dolg, M.; Wedig, U.; Stoll, H.; Preuss, H. Energy-adjusted *ab initio* pseudopotentials for the first row transition elements. *J. Chem. Phys.* **1987**, *86*, 866−872.
(27) (a) Miertuš, S.; Scrocco, E.; Tomasi, J. Electrostatic interaction of a solute with a continuum. A direct utilizaion of ab initio molecular potentials for the prevision of solvent effects. *Chem. Phys.* **1981**, *55*, 117−129. (b) Scalmani, G.; Frisch, M. Continuous surface charge polarizable continuum models of solvation. I. General formalism. *J. Chem. Phys.* **2010**, *132*, No. 114110.

https://doi.org/10.1021/acsomega.2c04645
ACS Omega 2022, 7, 36634−36642